AD-A174 698 COMPARISON OF OCEAN TIDE MODELS WITH SATELLITE ALTIMETER DATA(U) NAVAL RESEARCH LAB WASHINGTON DC L W CHOY ET AL 14 NOV 86 NRL-MR-5866 1/1

UNCLASSIFIED F/G 8/3 NL

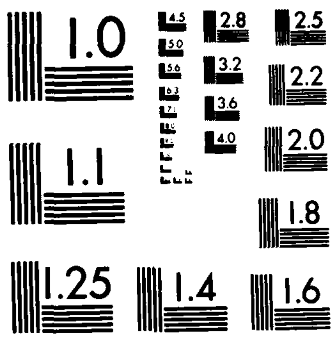

MICROCOPY RESOLUTION TEST CHART
NATIONAL BUREAU OF STANDARDS-1963-A

(2)

Naval Research Laboratory

Washington, DC 20375-5000 NRL Memorandum Report 5866 November 14, 1986

Comparison of Ocean Tide Models with Satellite Altimeter Data

L. W. CHOY AND M. R. GRUNES

Space Sensing Applications Branch
Space Systems and Technology Division

This project was funded by SPAWAR and the Office of Naval Research.

ADA174698

SECURITY CLASSIFICATION OF THIS PAGE

REPORT DOCUMENTATION PAGE

1a. REPORT SECURITY CLASSIFICATION: UNCLASSIFIED	1b. RESTRICTIVE MARKINGS
2a. SECURITY CLASSIFICATION AUTHORITY	3. DISTRIBUTION/AVAILABILITY OF REPORT: Approved for public release; distribution unlimited.
2b. DECLASSIFICATION / DOWNGRADING SCHEDULE	
4. PERFORMING ORGANIZATION REPORT NUMBER(S): NRL Memorandum Report 5866	5. MONITORING ORGANIZATION REPORT NUMBER(S)
6a. NAME OF PERFORMING ORGANIZATION: Naval Research Laboratory; 6b. OFFICE SYMBOL (If applicable)	7a. NAME OF MONITORING ORGANIZATION
6c. ADDRESS (City, State, and ZIP Code): Washington, DC 20375-5000	7b. ADDRESS (City, State, and ZIP Code)
8a. NAME OF FUNDING/SPONSORING ORGANIZATION: SPAWAR and ONR; 8b. OFFICE SYMBOL (If applicable)	9. PROCUREMENT INSTRUMENT IDENTIFICATION NUMBER
8c. ADDRESS (City, State, and ZIP Code): Washington, DC 20361 Arlington, VA 22217	10. SOURCE OF FUNDING NUMBERS: PROGRAM ELEMENT NO. (See page ii); PROJECT NO.; TASK NO.; WORK UNIT ACCESSION NO.

11. TITLE (Include Security Classification)

Comparison of Ocean Tide Models with Satellite Altimeter Data

12. PERSONAL AUTHOR(S)

Choy, L. W. and Grunes, M.

13a. TYPE OF REPORT	13b. TIME COVERED	14. DATE OF REPORT (Year, Month, Day)	15. PAGE COUNT
Final	FROM 1/85 TO 7/86	1986 November 14	24

16. SUPPLEMENTARY NOTATION

This project was funded by SPAWAR and the Office of Naval Research.

17. COSATI CODES			18. SUBJECT TERMS (Continue on reverse if necessary and identify by block number)
FIELD	GROUP	SUB-GROUP	Satellite altimetry; Ocean tide models; SEASAT altimetry

19. ABSTRACT (Continue on reverse if necessary and identify by block number)

Ocean tides are noise to those who wish to construct the ocean geoid using satellite altimeter data. Precise modeling of the ocean tides will help improve the geoid modeling accuracy. This report studies whether altimeter data itself can be used to assess various tide models. The Schwiderski Global Ocean Tide Model and the Kuo Pacific Ocean tide model were examined using SEASAT altimeter data in the Gulf of Alaska and South Pacific region. The feasibility of using altimeter data to assess tide models is demonstrated.

20. DISTRIBUTION/AVAILABILITY OF ABSTRACT: ☒ UNCLASSIFIED/UNLIMITED ☐ SAME AS RPT. ☐ DTIC USERS	21. ABSTRACT SECURITY CLASSIFICATION: UNCLASSIFIED
22a. NAME OF RESPONSIBLE INDIVIDUAL: L. W. Choy	22b. TELEPHONE (Include Area Code): (202) 767-2778; 22c. OFFICE SYMBOL: Code 7785.1

DD FORM 1473, 84 MAR — 83 APR edition may be used until exhausted. All other editions are obsolete.

SECURITY CLASSIFICATION OF THIS PAGE

10. SOURCE OF FUNDING NUMBERS

PROGRAM ELEMENT NO.	PROJECT NO.	TASK NO.	WORK UNIT ACCESSION NO.
63207N	X 0527		DN680-370
61153N	RR032-01-01		DN330-057

CONTENTS

COMPARISON OF OCEAN TIDE MODELS WITH SATELLITE ALTIMETER DATA

I. INTRODUCTION

The marine geoid is a gravitational equipotential surface which nearly coincides with the mean sea surface. Mapping the mean sea surface with respect to the reference ellipsoid is one method of determining the geoid of the ocean. On a global scale, satellite altimetry is an excellent and perhaps the only practical tool, at present and in the near future, for mapping the marine geoid. Figure 1 illustrates the observational configuration of satellite altimetry over the ocean. The radar altimeter is a range (distance) measuring device. A pulse of electromagnetic energy is emitted from a transmitter and the reflected pulse is analyzed by a receiver. The distance from the altimeter to the target is determined by measuring the two-way travel time of the pulse. The error in the determination of the mean sea surface topography has contributions from uncertainties in (1) orbit determination, (2) instrument calibration, (3) propagation delay due to the electron density in the ionosphere and water content in the atmosphere, (4) bias introduced into the range measurement due to the presence of wind waves on the sea surface (the so-called electromagnetic bias) [Choy et al., 1983], and (5) temporal variations of sea height due to storm surges, currents, and ocean tides. This last error source, the temporal variations of the sea height from the mean sea surface, can be removed either by long term averaging of the data or accounted for by ocean models. The SEASAT altimeter (instrument) range measurement noise was a function of the ocean surface wave height, varying between 5 and 10 cm for significant wave heights less than 5 m [Townsend, 1980].

Of the various types of ocean modeling, tide modeling probably has the longest history. Although the driving forces for tides have been accurately known for a long time, the equations governing tidal currents essentially being those of gravity and classical hydrodynamics, the exact solution of the tidal equations has been hindered by the inability to realistically apply boundary conditions. Idealized models had to be constructed and approximation methods tried.

Since Newton's time, efforts to model tides have been grouped into three categories [Schwiderski, 1980]: (1) Empirical methods, extrapolating tidal observations both in space and in time; (2) theoretical methods, solving the tidal equations using idealized boundary conditions and approximations; and (3) hydrodynamical interpolation methods, combining (1) and (2). Because of the importance of a tide correction for altimeter measurements, the question was asked whether altimeter data itself could be used to assess various tide models. Two models of interest to the Office of Naval Research (ONR) were the Schwiderski Global Ocean Tide Model in the frequency domain [Schwiderski, 1980, Schwiderski and Szeto, 1981], and the Global Tide Model in the time domain that was being developed at Columbia

Manuscript approved August 7, 1986

University by Professor John Kuo and his associates. Professor Kuo's model has recently been published [Kuo, et al. 1985]. The Schwiderski Global Ocean Tide Model fits the third category mentioned above by means of the finite differences method and constrained by tidal observations. Kuo's model is based solely on solving the vertically integrated hydrodynamic equations, i.e., including the advective term, with a rigid boundary condition at the artificially terminated boundaries, and without any constraints of tidal observations. Kuo's model used a semi-implicit scheme, finite element in space, and finite difference in time. This paper reports the comparison of these two models with SEASAT altimeter data in the Gulf of Alaska and South Pacific region.

II. DATA SOURCES

The SEASAT-1 altimeter data were obtained from the Naval Surface Weapons Center (NSWC), Dahlgren, Virginia. These data had been pre-processed at NSWC into the NSWC Geophysical Data Record (GDR) format [West, 1981]. In addition to the basic altimeter scientific data at a rate of approximately one per second, the GDR contains tide heights from the NSWC (Schwiderski) Global Ocean Tide Model computed along the sub-satellite tracks. The NSWC precise TRANET doppler orbital ephemerides, which have an accurancy of ~1.5 meter in the radial direction, were used throughout this work. Tide heights from Kuo's tide model computed along selected SEASAT passes were obtained from Professor Kuo at Columbia University. Kuo's model is based on the calculation of a Pacific Ocean model, which is bounded by Latitudes 60°N and 60°S, and Longitudes 60°W and 230°W only. Because of the artificially terminated boundaries at Latitude 60°S, the tidal height distribution in the southern Pacific Ocean is considerably different from that of a truly global ocean model, extending to Antartica and including the Atlantic and Indian Oceans. Kuo, et al. (1985) found that the interflows of the tidal induced currents between the Pacific Ocean and the Atlantic and Indian Oceans as well as the Arctic Ocean have a profound influence on the general tidal circulations as functions of space and time and introduce both phase shifts and amplitude changes.

The SEASAT (near 3-day exact repeat) passes used are summarized in Table 1.

III. METHOD OF ANALYSIS

At present, in order to use satellite altimetry to measure dynamic sea surface topographies, which have a height variation range of one meter or less over a horizontal distance of 100 Km or more, the orbit and geoid uncertainty problems must be resolved. Since SEASAT satellite orbit determination and the available geoid model in the Gulf of Alaska region have uncertainties greater than the tidal signals we wished to observe, comparisons of altimeter profiling data from a single pass over the ocean with tide models were not fruitful. Fortunately, during the last part of the SEASAT mission, the satellite was placed into a three-day near repeat orbit. Since the geoid is essentially time invariant in the time scale of our interest, a temporal change of sea surface height along the track was obtained by differencing the altimeter height data of two passes over an

TABLE 1
SEASAT PASSES USED IN THE TIDE MODEL COMPARISON

		START			END		
PASS #	YYDDD	SEC	LAT(N)	LON(E)	SEC	LAT(N)	LON(E)
1177	78260	27857	44.1	235.7	29816	-63.3	169.1
1220	78263	28621	44.1	235.7	30582	-63.3	169.1
1263	78266	29387	44.1	235.7	31347	-63.3	169.1
1191	78261	26256	35.4	238.4	28060	-63.5	177.2
1234	78264	27020	35.4	238.4	28826	-63.5	177.1
1277	78267	27785	35.5	238.4	29591	-63.5	177.1
1192	78261	31941	54.6	228.6	34124	-64.3	150.2
1235	78264	32707	54.6	228.6	34890	-64.3	150.1
1278	78267	33472	54.6	228.6	35656	-64.3	150.1
1193	78261	37621	69.6	239.8	39776	-44.9	150.1
1236	78264	38387	69.8	239.7	40543	-45.0	150.1
1279	78267	39153	69.8	239.7	41308	-45.0	150.1
1207	78262	36126	59.5	218.5	38191	-54.1	150.1
1250	78265	36893	59.5	218.4	38957	-54.1	150.1
1293	78268	37658	59.5	218.4	39722	-54.1	150.1
1249	78265	31056	49.0	231.2	33129	-64.3	158.6
1292	78268	31821	49.0	231.2	33894	-64.3	158.6
1178	78260	33647	57.3	223.6	35791	-60.2	150.1
1221	78263	34415	57.2	223.4	36556	-60.2	150.1
1264	78266	35180	57.2	223.4	37322	-60.2	150.1

PASS # = SEASAT PASS #
YYDDD = YEAR, JULIAN DAY OF YEAR (1 = JAN. 1)
SEC = SECONDS OF DAY
LAT(N) = LATITUDE, DEGREES NORTH
LON(E) = LONGITUDE, DEGREES EAST

identical ground track, after the height and tide data for the second pass had been interpolated along the track to match the positions of the first pass.

The orbit error in SEASAT has been found to have a long wavelength of approximately one cycle per revolution [Colquitt, et al. 1980]. This introduced a tilt and curvature error in the altimeter profiling data. By choosing a long segment of a pass (about 1/3 of a revolution), the long wavelength orbit error was minimized by subtracting a second order polynomial least-squares fit with respect to time from the altimeter height difference data. By doing so we also removed the long wave length component of the tide difference as well. To place the tide model difference on the same footing, we also made a second order polynomial fit to the tide model difference and subtracted the fit out before comparisons were made. After removing a second order polynomial fit from the data, the sea surface height difference of a pair of coincident altimeter passes is referred to as the residual sea surface height difference (HDIFA) and the tide model height difference is referred to as the residual tide model difference (TDIFA). As will be seen, tide height differences with wavelenths of 16,000 km or smaller were easily observed by the altimeter.

IV. COMPARISON OF ALTIMETER DATA WITH TIDE MODELS

Figure 2A is a plot of the sub-satellite tracks of passes 1220 and 1263 as SEASAT traversed from the Gulf of Alaska to the South Pacific. As an illustration of the data analysis steps followed, Figure 2B is a plot of the one second averaged altimeter sea surface heights observed on these two passes. The fine geoidal features in these coincident passes nearly superimpose on each other. The vertical scale is in meters and the horizontal scale is in degrees of longitude. The same units are kept in subsequent figures for easy cross referencing. Plots of Schwiderski's and Kuo's model tide heights along these two sub-satellite tracks are shown in Figures 2C and 2D. The stepwise appearance in Figure 2D was due to the finite quantization of Kuo's data. Figures 3A and 3B are comparisons of sea surface height difference with the tide model height difference. The smooth curves are from tide model values and the noisy curves are from one second averaged altimeter data as contained in the NSWC SEASAT Geophysical Data Record. The residual sea surface height difference and residual Schwiderski and Kuo tide model height difference are shown in Figures 3C and 3D respectively. Both models compared favorably with the altimeter data in the open ocean for passes 1220 and 1263. The track length available was somewhat longer than the span used. The plots were restricted to match the positions supplied to us for Kuo's model.

The results of passes 1192 and 1235 are shown in Figure 4. These two coincident passes, 3 days apart in time, were further west than passes 1220 and 1263 discussed earlier. Schwiderski's model had a better agreement with the altimeter data than Kuo's model in the open ocean, as can be seen from Figures 4B and 4C.

A comparison for coincident passes 1192 and 1278 (about 6 days apart in time) and for coincident passes 1235 and 1278 (about 3 days apart in time) is shown in Figure 5. Here, Schwiderski's and Kuo's models showed a comparable agreement with the altimeter data in the northern Pacific Ocean; Schwiderski's model showed a better agreement in the southern Pacific Ocean with the altimeter data than Kuo's model. Professor Kuo suggested that these results are to be expected as Schwiderski's model is a global ocean model while Kuo's model has an artificially terminated boundary at latitude 60°S and thus introduces error in the computation of tidal heights in the southern Pacific Ocean.

This completes the Kuo model comparison since those were all the tide model heights provided to us by Columbia University.

Figures 6-12 are comparisons of altimeter data with Schwiderski's tide model only.

The trajectory of a group of three coincident passes 1177, 1220, and 1263 is shown in Figure 6A. Altimeter data south of about 65°S latitude were not used due to possible sea ice presence (contamination). Figures 6B, 6C, and 6D compare the residuals of Schwiderski's tide model with the altimeter data. The overall agreement was good in the open ocean. At 235.7°E longitude, near the Washington coast, the large coastal tide differences computed from the tide model were not observed in the altimeter data. However, coastal tide heights vary over a much greater range for a small horizontal distance than open ocean tides. A small orbital error in the subsatellite track can introduce large errors in the residual comparison in coastal waters. Actually, the orbit used by Schwiderski to compute the tides along the SEASAT track was not the same precise orbit computed for the NSWC GDR of the altimeter data. The NSWC "standard" orbit Schwiderski used differs by as much as 1° in latitude/longitude when compared to the NSWC precise orbit [Smith and Schwiderski, NSWC 1985]. It should also be pointed out that the other short wavelength temporal variations of sea height that are observed by the altimeter, including variations due to storm surge, currents, atmospheric and ionospheric disturbances, have not been accounted for in this work.

The tide model comparison for pass pairs 1191,1234; 1191,1277; 1234,1277; 1192,1235; 1192,1278; and 1235,1278 are shown in Figures 7 and 8. Notice that the overall agreement was quite good even near the coasts. The altimeter residual showed a somewhat greater tidal variation near the peak and trough areas than that computed by the tide model (Figures 7C, 7D, 8B, and 8C).

The tide model comparisons for pass pairs 1193,1236; 1193,1279; and 1236,1279 are shown in Figure 9. There was some fine structure in the tide model residual produced by the model near New Caledonia (165°E longitude). This fine structure was also observed by the altimeter.

The comparison for pass pairs 1207,1250; 1207,1293; and 1250,1293 are shown in Figure 10. Again, the overall agreement was excellent. Figure 11 is a comparison for pass pair 1249 and 1292. The altimeter residual again showed greater variation near the peak and trough areas than that computed by the tide model.

The comparison for pass pairs 1178,1221; 1178,1264; and 1221,1264 are shown in Figure 12. These passes crossed the northern tip of New Zealand at about 173°E longitude. The tide pile up of a meter or more across New Zealand (Figure 12B and 12C) was real (Sam Smith, NSWC, private communication) and the altimeter data followed it nicely. Between passes 1221 and 1264, both the tide model and the altimeter data showed a smooth transition.

V. SUMMARY AND CONCLUSION

The NSWC Ocean Tide Model contains nine harmonic partial tides of the semi-diurnal, (M_2, S_2, N_2, K_2), diurnal, (K_1, O_1, P_1, Q_1) and long-period (mf) species. The model includes effects of tide-generated terrestrial and oceanic mass perturbations. The Kuo model is a Pacific Ocean total tide model with earth tide corrections. The NSWC Ocean Tide Model has been published and is available on tape from NSWC, Dahlgren, VA. The Kuo Model has recently been published [Kuo et al., 1985].

The method employed here cannot ~~be~~ as yet be used to study the long wavelength component of tides removed by the quadratic fits, and only height differences along near-repeat sub-satellite tracks can be studied; if the altimeter repeat ground tracks do not overlap exactly, geoidal variations can not be completely removed by simple subtraction. The precision of satellite altimetry also places a limit on the accuracy with which one can safely assess the error of a tide model. Within these limitations, the feasibility of using altimeter data to assess tide models has been successfully demonstrated.

VI. ACKNOWLEDGMENTS

Support and encouragement given by Mr. John Heacock (Office of Naval Research) is gratefully acknowledged. There was much delay in writing this final report although the results had been previously communicated to the principal parties. At first there was a delay in receiving the tide model output from Professor Kuo. When the output finally arrived, key personnel had been reassigned to other tasks and the funding for the work had expired. We greatly appreciate Mr. Heacock's patience and understanding in this matter.

We would like to thank S. Smith and G. West of NSWC for providing us with the SEASAT data and for much help during many subsequent discussions. Professor John Kuo and his associate, Dr. Yu-Hua Chu, have been extremely cooperative and courteous and for this we thank them. Both Dr. Schwiderski and Professor Kuo have reviewed this work. Their constructive comments were deeply appreciated.

Richard Whitman II, Enzo Uliana, and Joseph Shuhy have made significant contributions to this effort. Our thanks also to Peter Mitchell for reviewing and to Linda Ridgely for typing the entire manuscript. Finally, we would like to thank Dr. Vincent Noble for his continued guidance and support. This task was supported in part by ONR Code 1125GG under SPAWAR P.E. 61153N, Project No. RR-032-01-01 and in part by the ROMS Project, PE 63207N, Project No. X-0527.

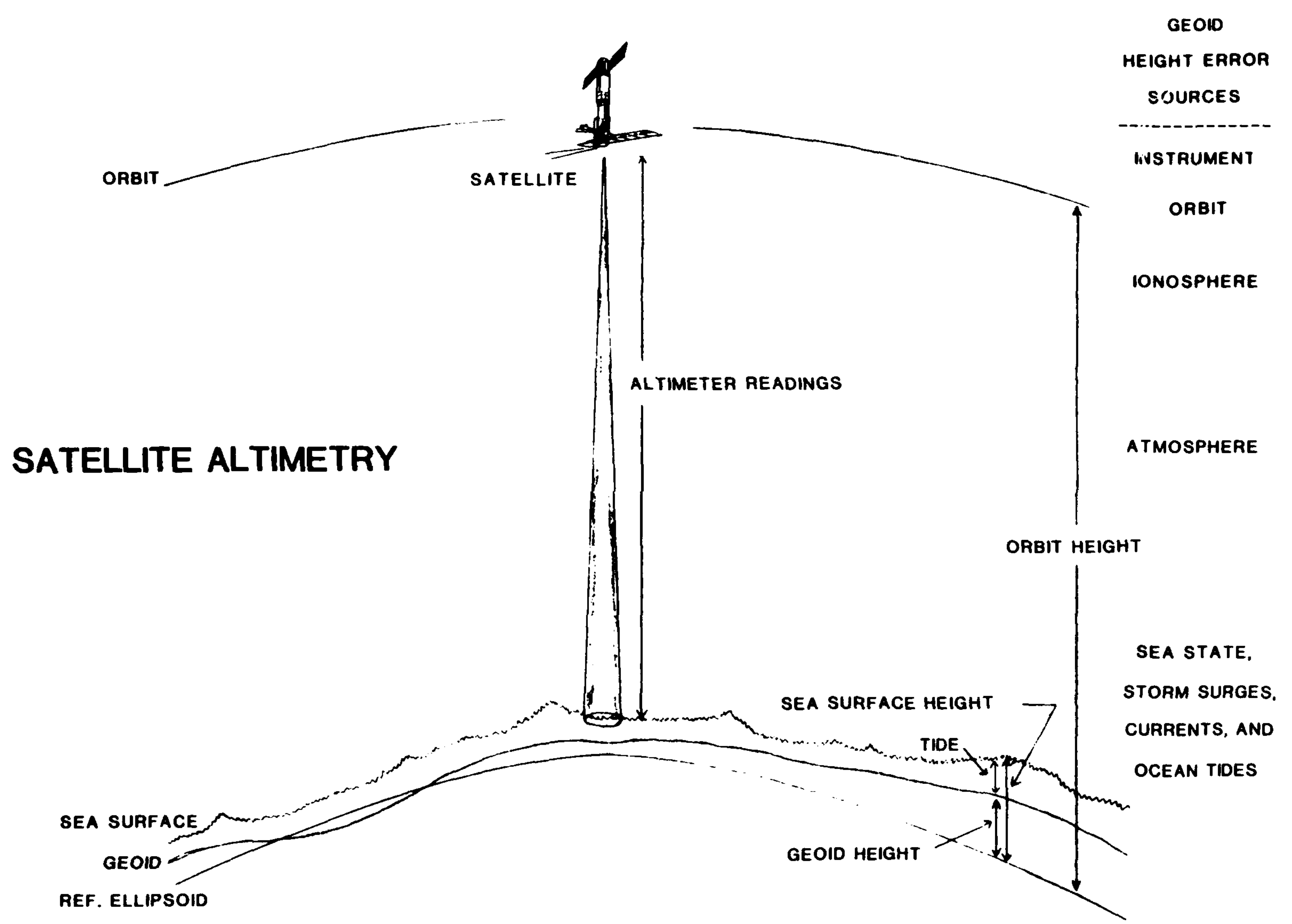

Fig. 1 — Satellite altimetry observation configuration

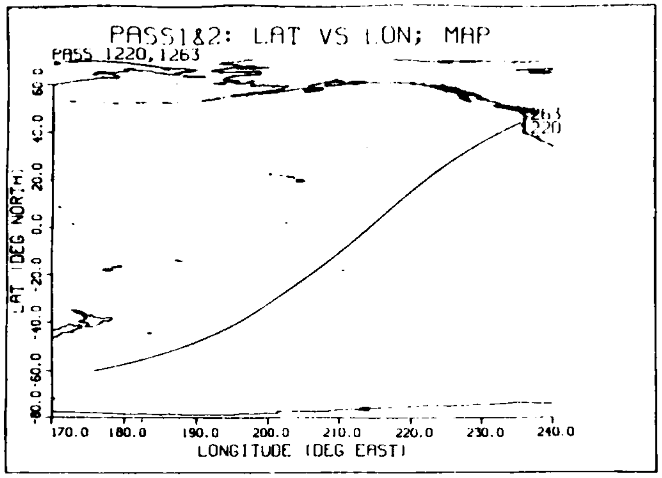

Fig 2A SEASAT orbital trajectory.

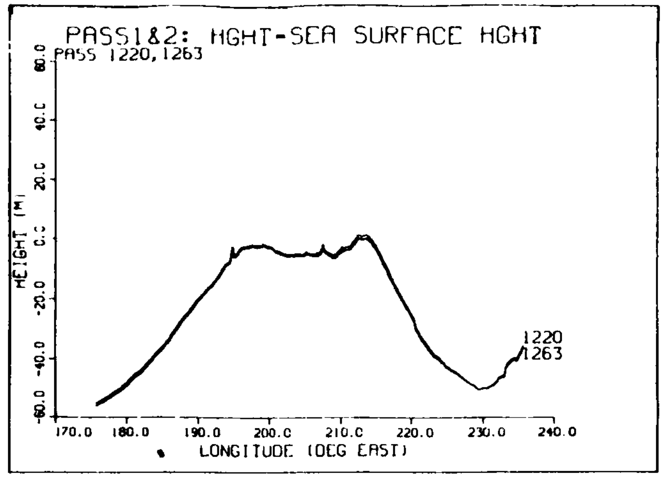

Fig 2B SEASAT sea surface heights over the reference ellipsoid.

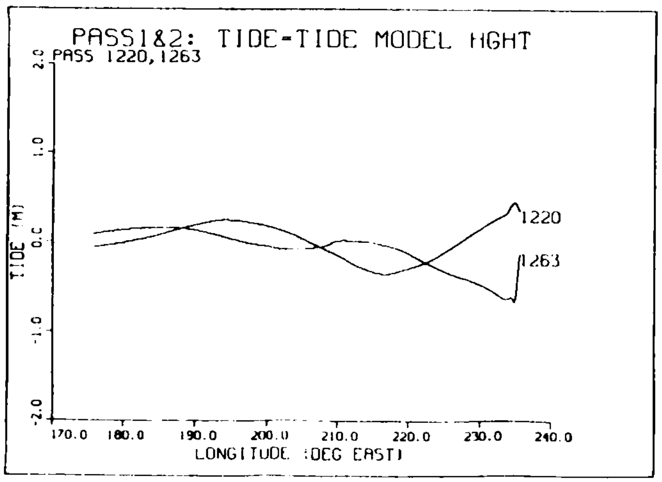

Fig 2C Schwiderski tide model heights.

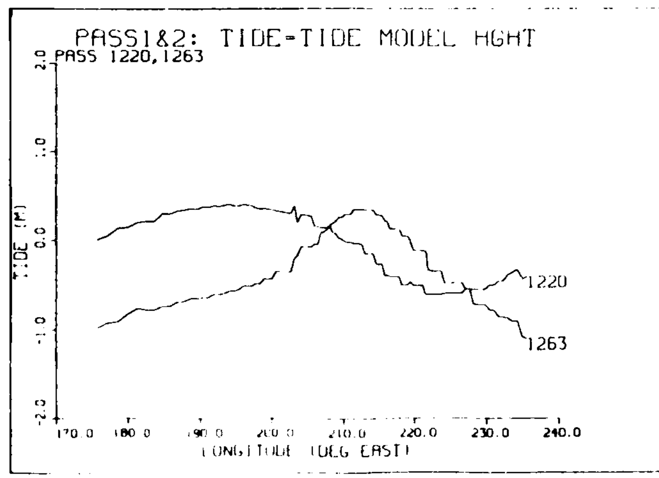

Fig 2D Kuo tide model heights.

Fig. 2 — Trajectory, height and tide data for SEASAT coincident passes 1220 and 1263. Data restricted to match positions of Kuo . data.

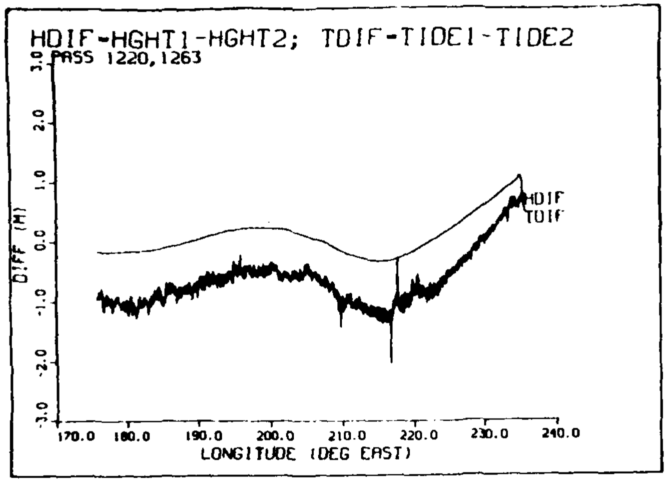

Fig 3A SEASAT sea surface height difference (lower curve) and and Schwiderski tide model difference.

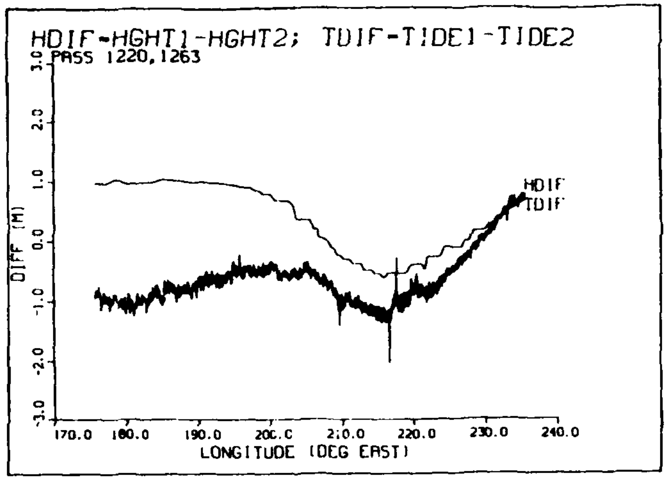

Fig 3B SEASAT sea surface height difference (lower curve) and Kuo tide model difference.

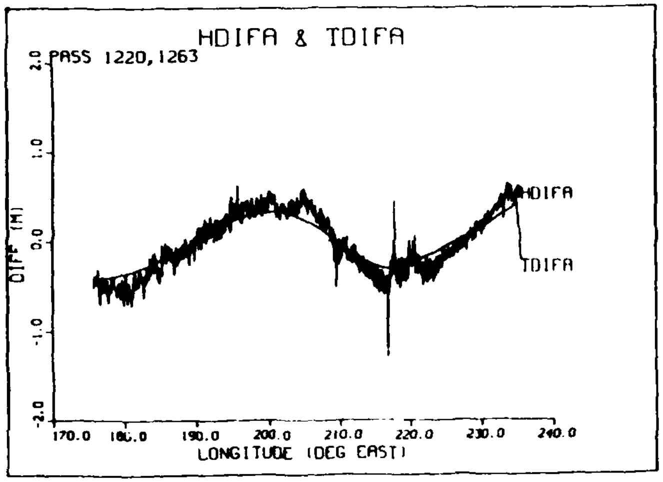

Fig 3C Residual SEASAT sea surface height difference and residual Schwiderski tide model difference.

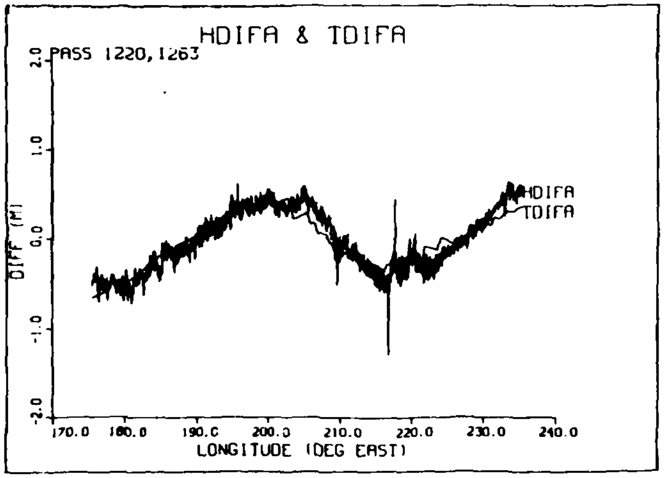

Fig 3D Residual SEASAT sea surface height difference and residual Kuo tide model difference.

Fig. 3 — Tide comparisons for SEASAT coincident passes 1220 and 1263.
Data restricted to match positions of Kuo's data.

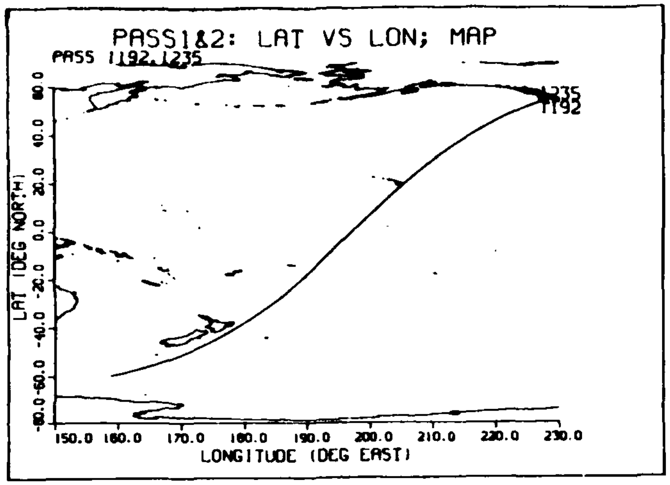

Fig 4A SEASAT orbital trajectory for passes 1192, 1235 and 1278.

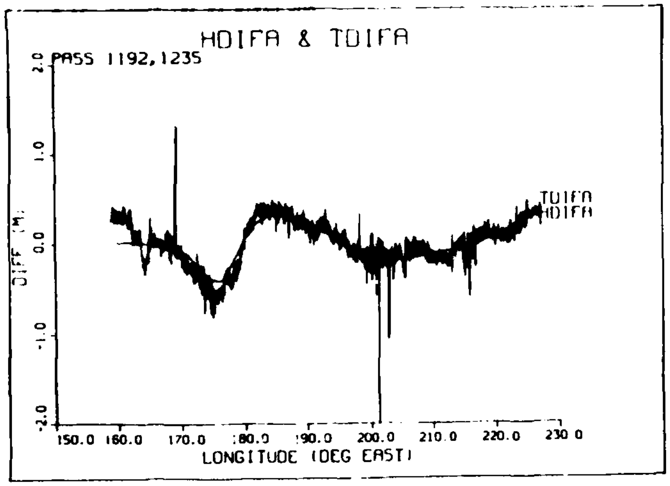

Fig 4B Residual SEASAT sea surface height difference and residual Schwiderski tide model difference.

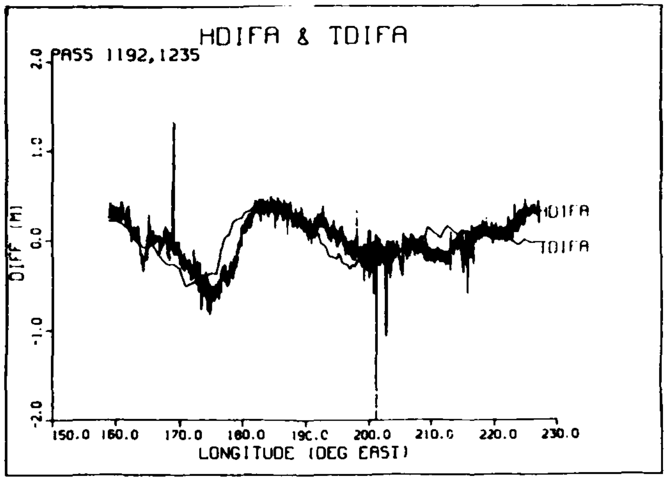

Fig 4C Residual SEASAT sea surface height difference and residual Kuo tide model difference.

Fig. 4 — Tide comparisons for SEASAT coincident passes 1192 and 1235. Data restricted to match positions of Kuo's data.

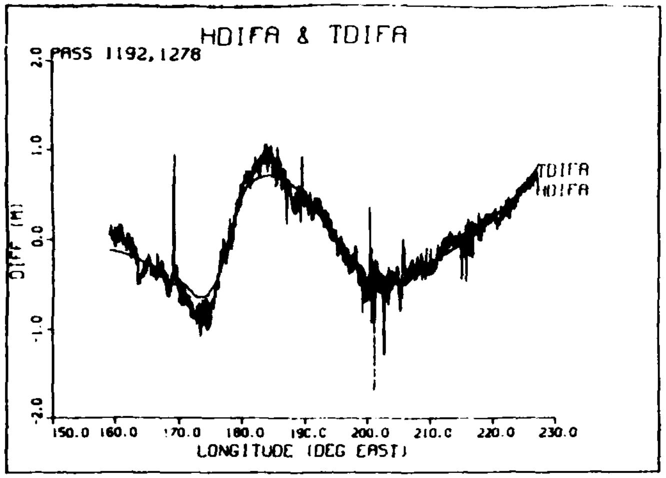

Fig 5A Residual SEASAT sea surface height difference and residual Schwiderski tide model difference for passes 1192 and 1278.

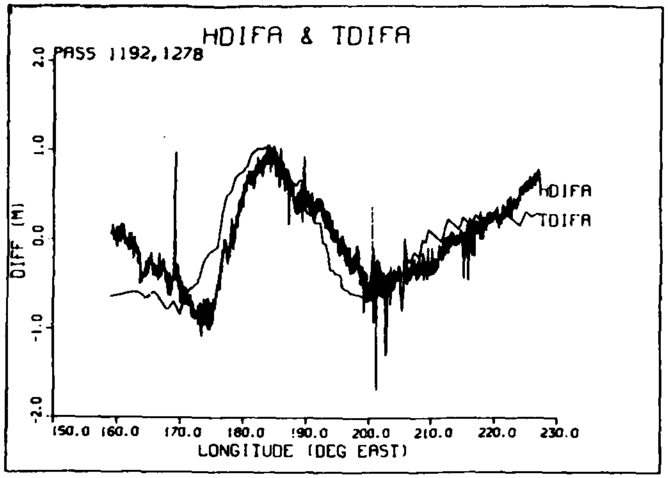

Fig 5B Residual SEASAT sea surface height difference and residual Kuo tide model difference for passes 1192 and 1278.

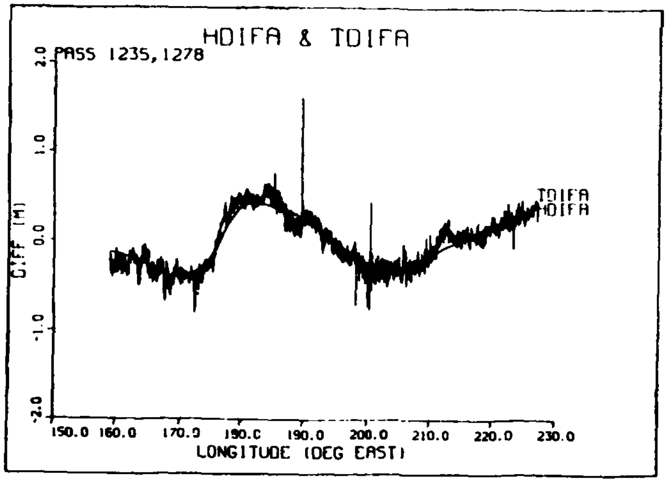

Fig 5C Residual SEASAT sea surface height difference and residual Schwiderski tide model difference for passes 1235 and 1278.

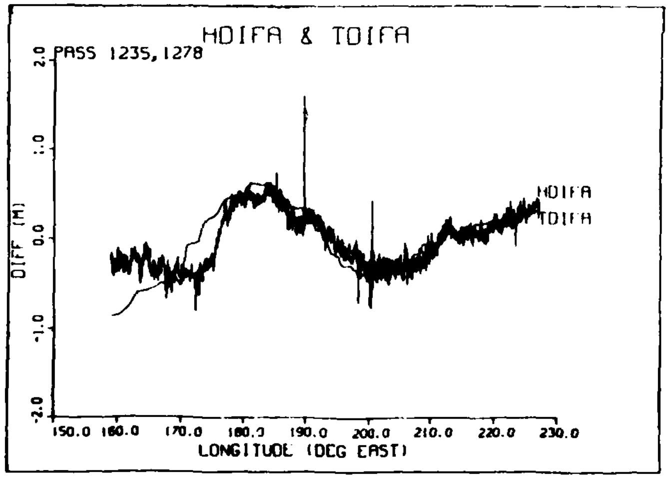

Fig 3D Residual SEASAT sea surface height difference and residual Kuo tide model difference for passes 1235 and 1278.

Fig. 5 — Tide comparisons for coincident passes 1192 and 1278, and for 1235 and 1278. Data restricted to match positions of Kuo's data.

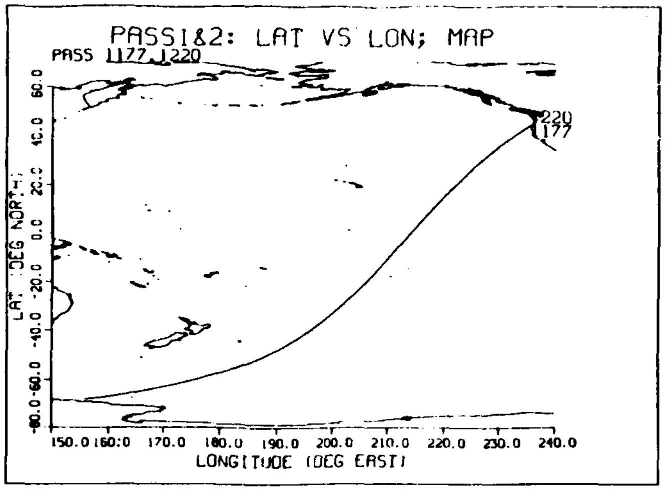

Fig 6A SEASAT orbital trajectory for passes 1177, 1220 and 1263.

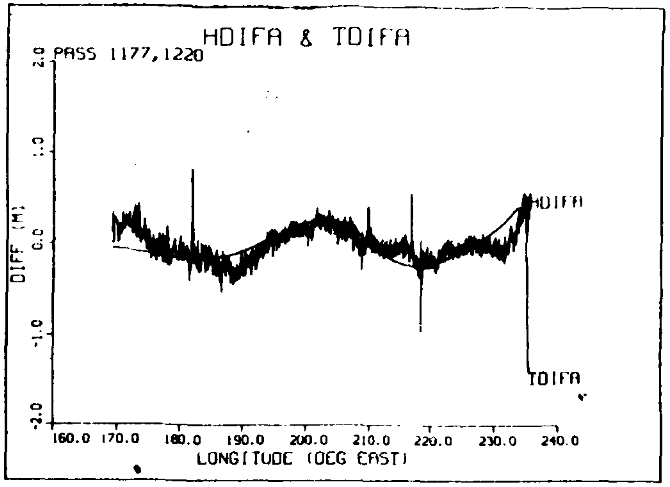

Fig 6B Residual SEASAT sea surface height difference and residual Schwiderski tide model difference for passes 1177 and 1220.

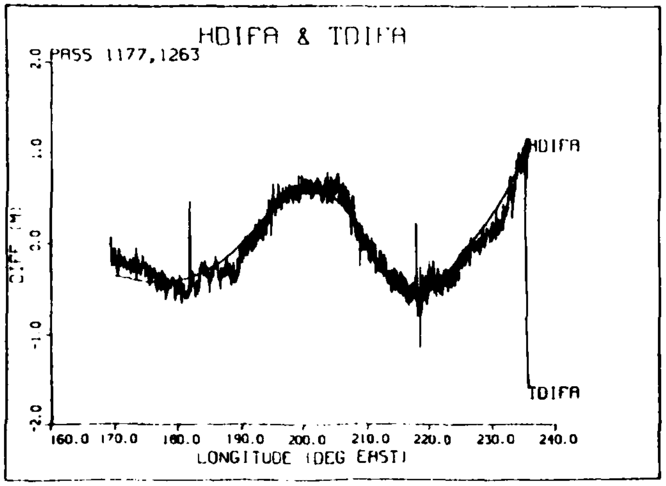

Fig 6C Residual SEASAT sea surface height difference and residual Schwiderski tide model difference for passes 1177 and 1263.

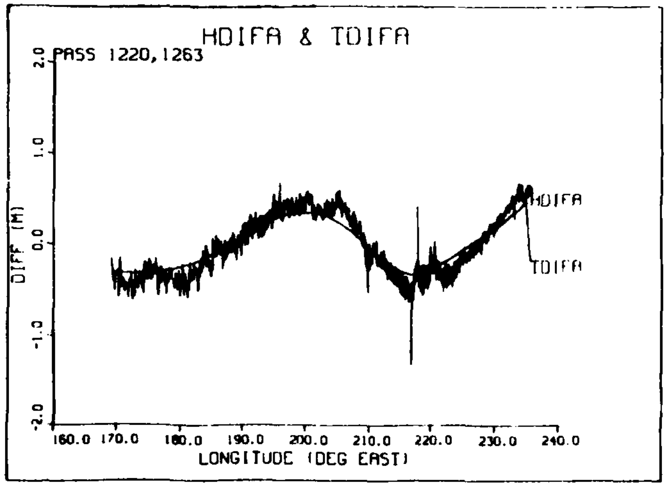

Fig 6D Residual SEASAT sea surface height difference and residual Schwiderski tide model difference for passes 1220 and 1263.

Fig. 6 — Tide comparisons for SEASAT coincident passes 1177, 1220 and 1263. Data restricted to avoid ice.

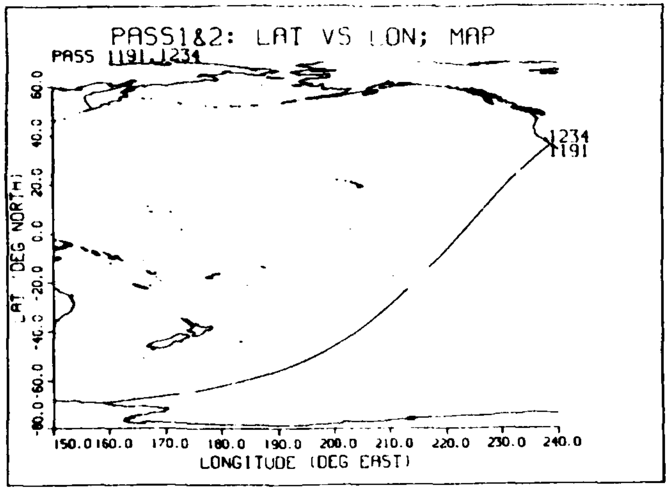

Fig 7A SEASAT orbital trajectory for passes 1191, 1234 and 1277.

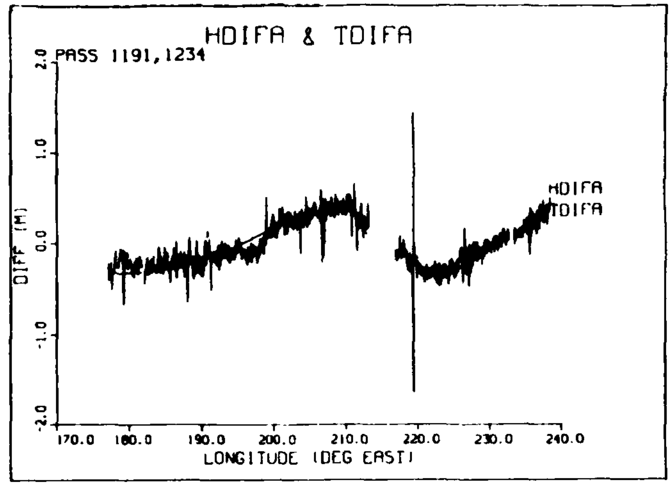

Fig 7B Residual SEASAT sea surface height difference and residual Schwiderski tide model difference for passes 1191 and 1234.

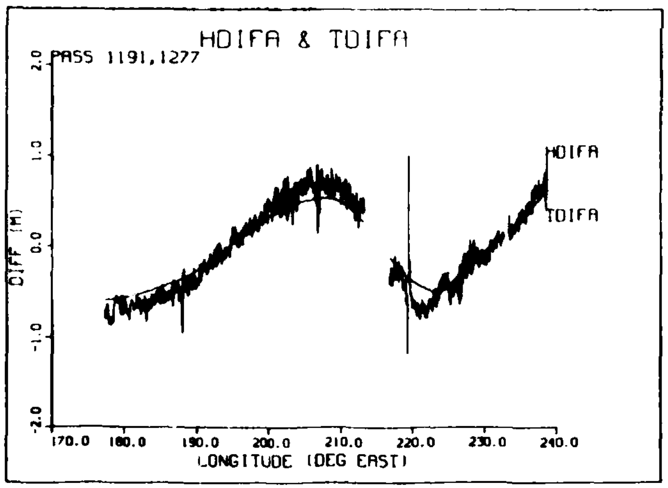

Fig 7C Residual SEASAT sea surface height difference and residual Schwiderski tide model difference for passes 1191 and 1277.

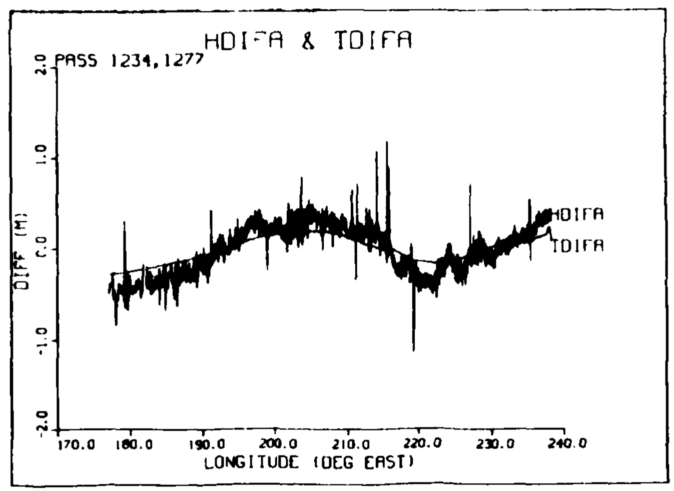

Fig 7D Residual SEASAT sea surface height difference and residual Schwiderski tide model difference for passes 1234 and 1277.

Fig. 7 — Tide comparisons for SEASAT coincident passes 1191, 1234 and 1277. Data restricted to avoid ice.

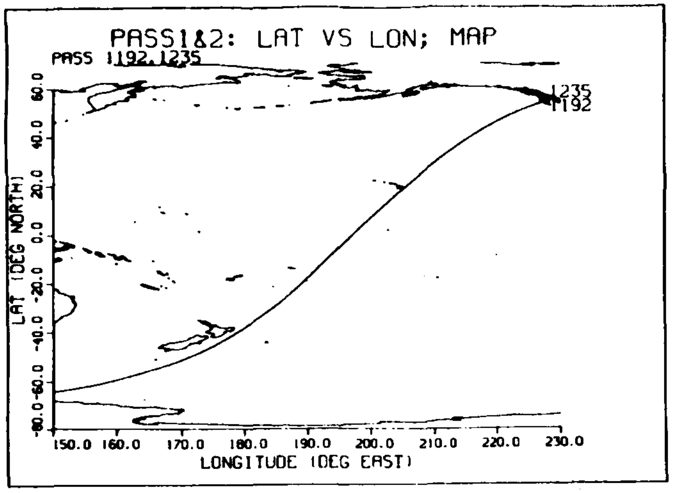

Fig 8A SEASAT orbital trajectory for passes 1192, 1235 and 1278.

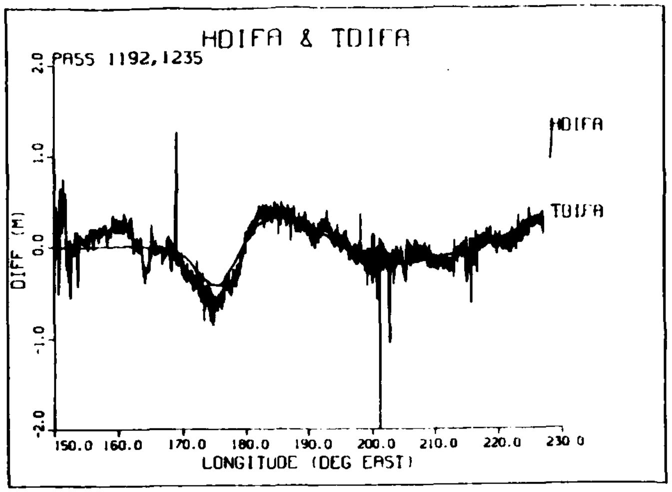

Fig 8B Residual SEASAT sea surface height difference and residual Schwiderski tide model difference for passes 1192 and 1235.

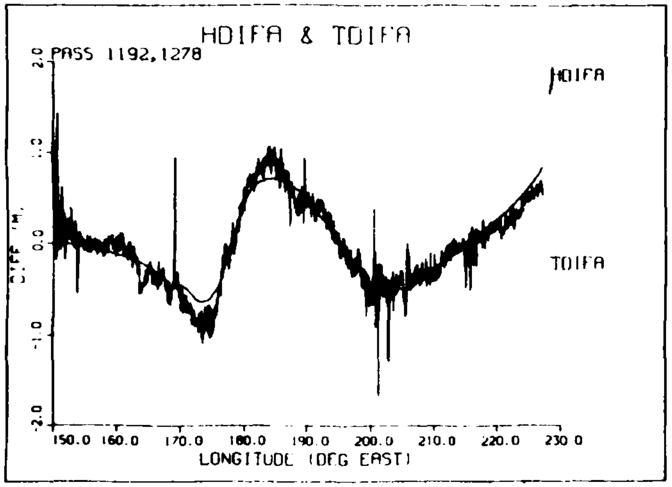

Fig 8C Residual SEASAT sea surface height difference and residual Schwiderski tide model difference for passes 1192 and 1278.

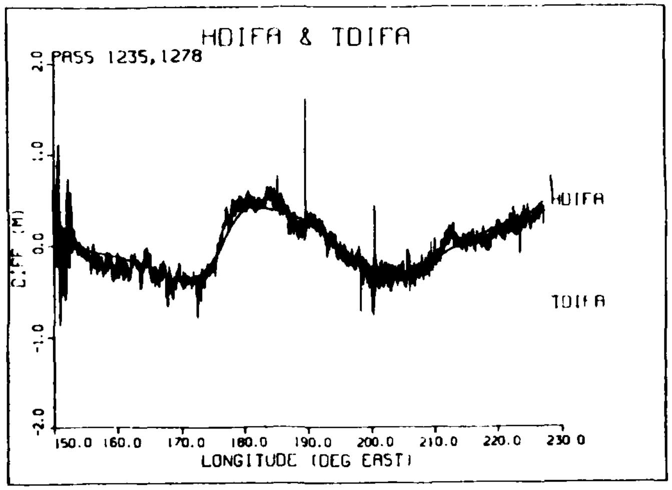

Fig 8D Residual SEASAT sea surface height difference and residual Schwiderski tide model difference for passes 1235 and 1278.

Fig. 8 — Tide comparison for SEASAT coincident passes 1192, 1235 and 1278

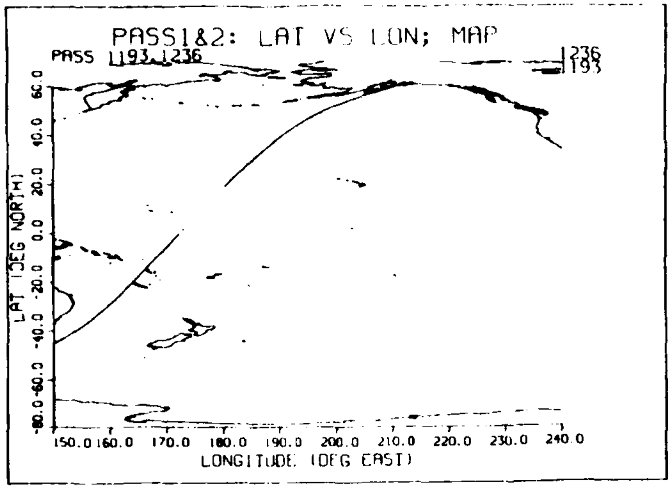

Fig 9A SEASAT orbital trajectory for passes 1193, 1236 and 1279.

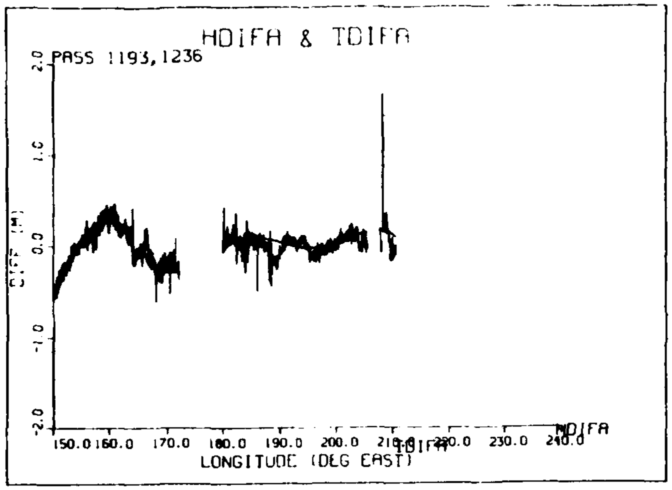

Fig 9B Residual SEASAT sea surface height difference and residual Schwiderski tide model difference for passes 1193 and 1236.

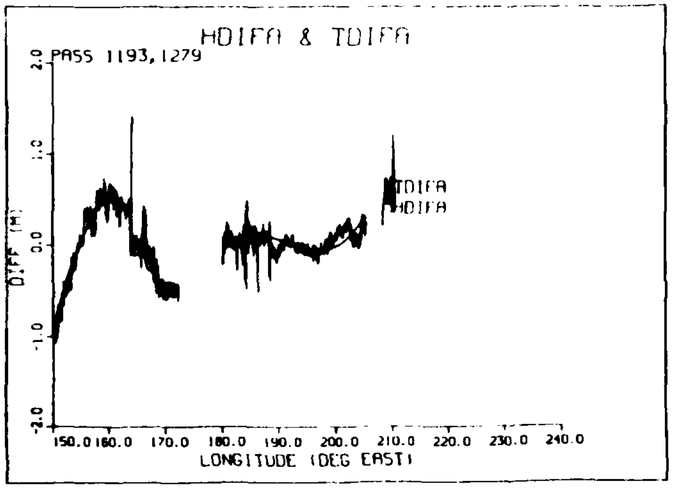

Fig 9C Residual SEASAT sea surface height difference and residual Schwiderski tide model difference for passes 1193 and 1279.

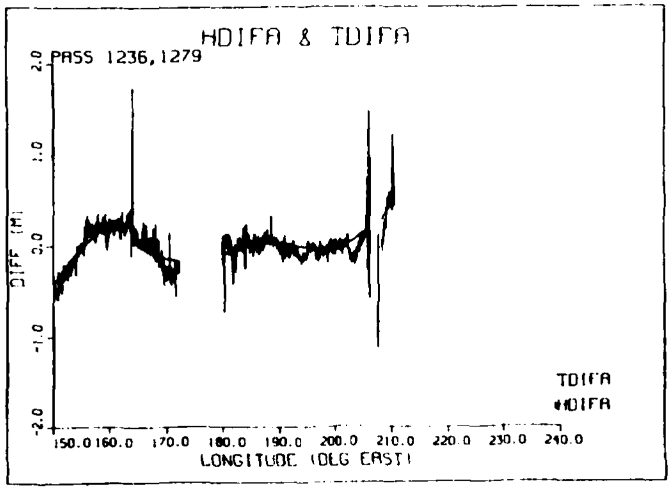

Fig 9D Residual SEASAT sea surface height difference and residual Schwiderski tide model difference for passes 1236 and 1279.

Fig. 9 — Tide comparison for SEASAT coincident passes 1193, 1236 and 1279

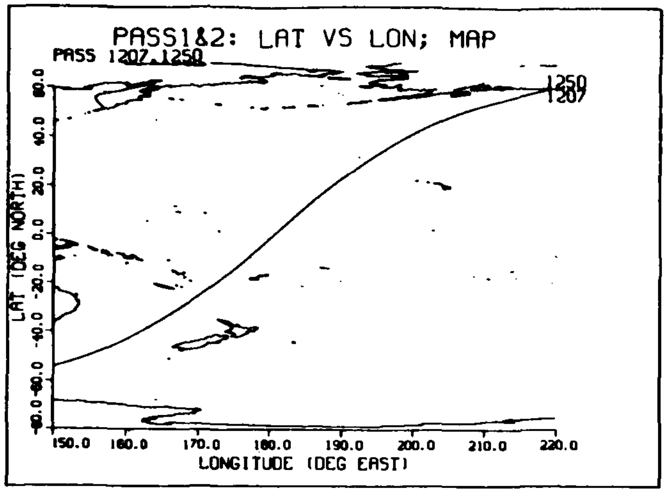

Fig 10A SEASAT orbital trajectory for passes 1207, 1250 and 1293.

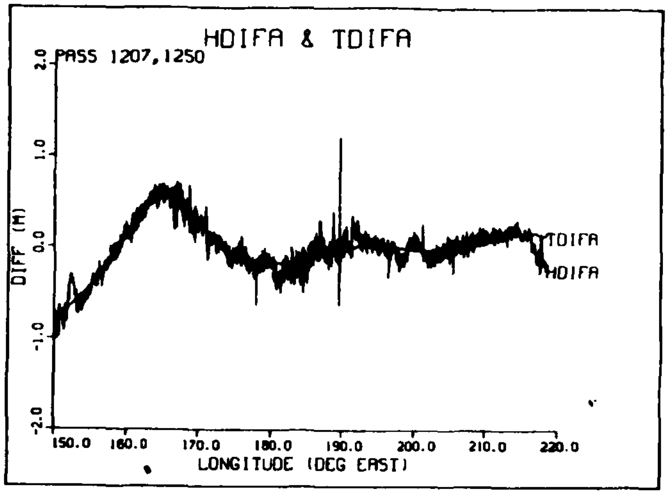

Fig 10B Residual SEASAT sea surface height difference and residual Schwiderski tide model difference for passes 1207 and 1250.

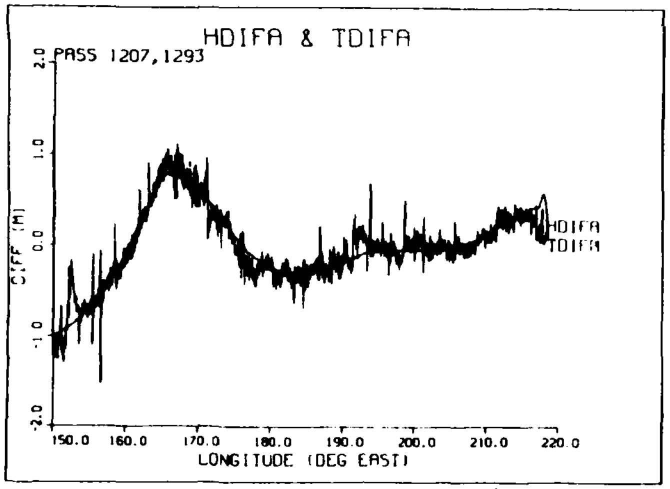

Fig 10C Residual SEASAT sea surface height difference and residual Schwiderski tide model difference for passes 1207 and 1293.

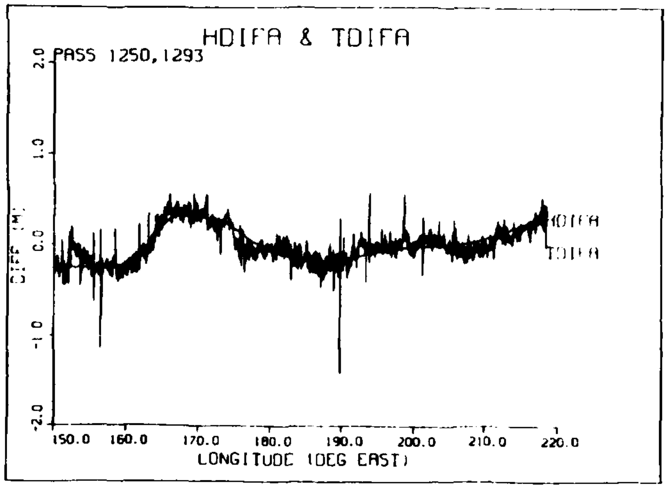

Fig 10D Residual SEASAT sea surface height difference and residual Schwiderski tide model difference for passes 1250 and 1293.

Fig. 10 — Tide comparison for SEASAT coincident passes 1207, 1250 and 1293

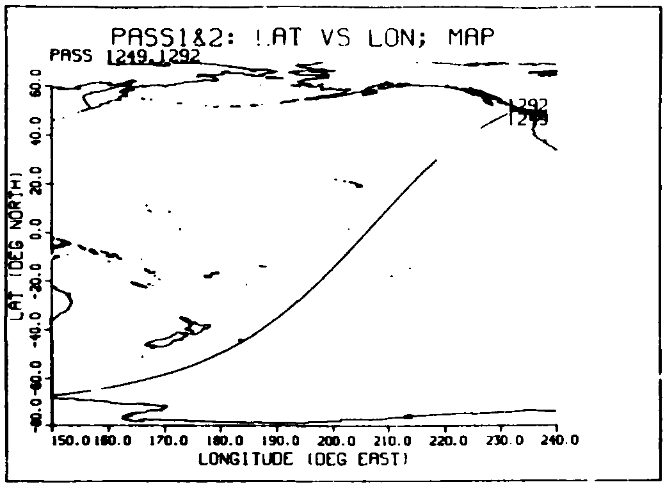

Fig 11A SEASAT orbital trajectory for passes 1249 and 1292.

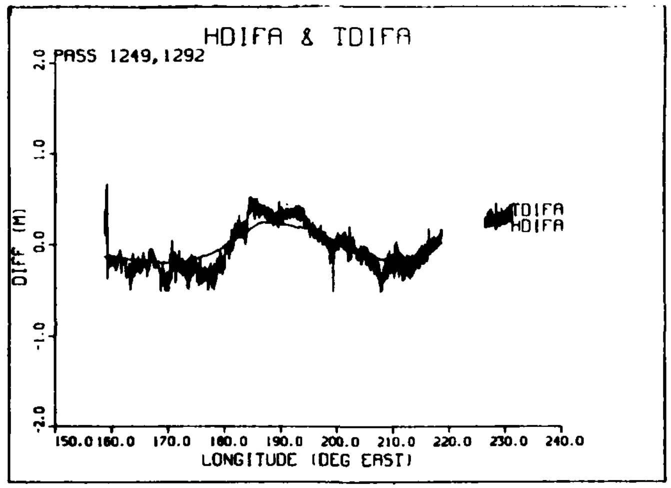

Fig 11B Residual SEASAT sea surface height difference and residual Schwiderski tide model difference for passes 1249 and 1292.

Fig. 11 — Tide comparisons for SEASAT coincident passes 1249 and 1292. Data restricted to avoid ice.

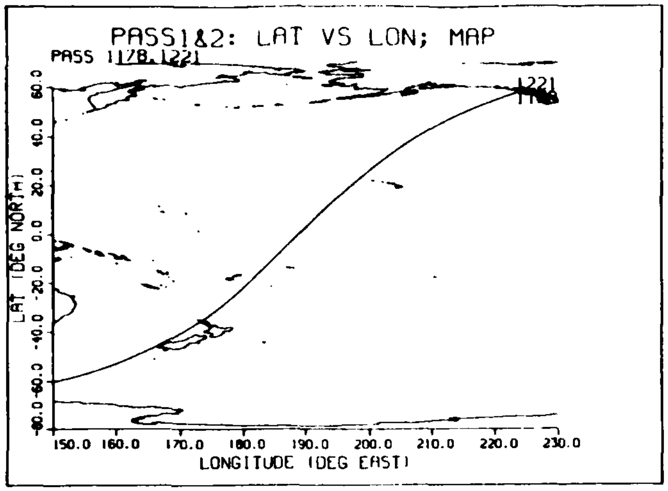

Fig 12A SEASAT orbital trajectory for passes 1178, 1221 and 1264.

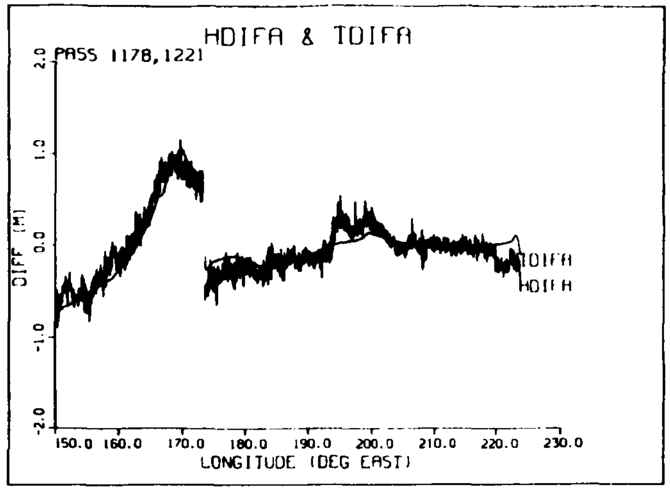

Fig 12B Residual SEASAT sea surface height difference and residual Schwiderski tide model difference for passes 1178 and 1221.

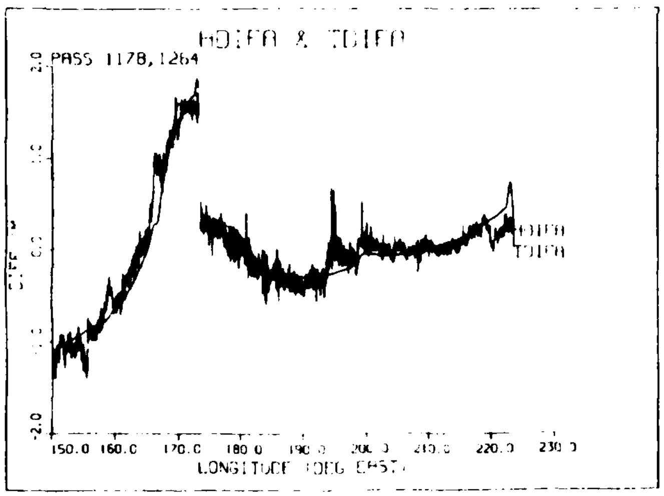

Fig 12C Residual SEASAT sea surface height difference and residu. Schwiderski tide model difference for passes 1178 and 1264.

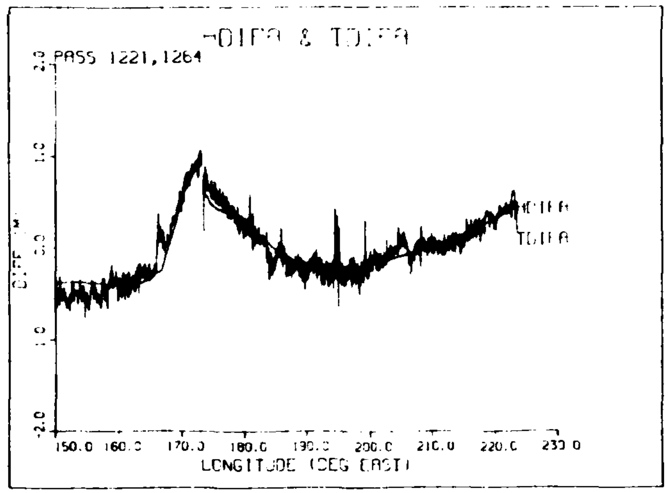

Fig 12D Residual SEASAT sea surface height difference and residual Schwiderski tide model difference for passes 1221 and 1264.

Fig. 12 — Tide comparisons for SEASAT coincident passes 1178, 1221 and 1264. Note correctly modeled ocean pileup across tip of New Zealand.

VII. REFERENCES

1. Colquitt, E. S., C. W. Malyevac, and R. J. Anderle, "Doppler Computed Seasat Orbits", J. of Astronautical Sciences, Vol. XXVIII, No. 4, pp. 391-403, Dec. 1980.

2. Choy, L. W., D. L. Hammond, and E. A. Uliana, "The Electromagnetic Bias of Altimeter Measurements of Mean Sea Level as Determined by an Airborne 10 GHz Radar", NRL Memorandum Report 5006, Jan. 1983. (AD-A123 234)

3. Kuo, J. T., Y. H. Chu, and N. M. Chen, "Time-Domain Finite Element Modeling of the Global Ocean Tides", Proceedings of the Tenth International Symposium on Earth Tides, September, 1985, Madrid, Spain.

4. Schwiderski, E. W., On Charting Global Ocean Tides, "Reviews of Geophysics and Space Physics", Vol. 18, No. 1, pp. 243-268, February 1980.

5. Schwiderski, E. W. and L. T. Szeto, "The NSWC Global Ocean Tide Data Tape (GOTD) Its Features and Application Random-Point Tide Program", NSWC TR 81-254, June 1981. (AD-A105 974)

6. Smith, S. and E. Schwiderski, 1985, Private Communication.

7. Townsend, W. F., "An Initial Assessment of the Performance Achieved by the SEASAT-1 Radar Altimeter", IEEE J. of Ocean Engineering, Vol. OE-5, No. 2, April 1980, pp. 80-92.

8. West, G. B., "SEASAT Satellite Radar Altimetry Data Processing System", Naval Surface Weapons Center Technical Report NSWC TR81-234, May 1981. (AD-A115 972)

END

1-87

DTIC